

Effects of In Vivo Mechanical Loading on Large Bone Defect Regeneration

Joel D. Boerckel,^{1,2} Yash M. Kolambkar,³ Hazel Y. Stevens,^{1,2} Angela S.P. Lin,^{1,2} Kenneth M. Dupont,^{1,2} Robert E. Guldberg^{1,2,3}

¹Institute for Bioengineering and Bioscience, Georgia Institute of Technology, Atlanta, Georgia, ²Woodruff School of Mechanical Engineering, Georgia Institute of Technology, Atlanta, Georgia, ³Coulter Department of Biomedical Engineering, Georgia Institute of Technology, Atlanta, Georgia

Received 6 June 2011; accepted 21 November 2011

Published online in Wiley Online Library (wileyonlinelibrary.com). DOI 10.1002/jor.22042

ABSTRACT: Fracture healing is highly sensitive to mechanical conditions; however, the effects of mechanical loading on large bone defect regeneration have not been evaluated. In this study, we investigated the effects of functional loading on repair of critically sized segmental bone defects. About 6-mm defects were created in rat femora, and each defect received 5 μ g recombinant human bone morphogenetic protein-2 (rhBMP-2), delivered in alginate hydrogel. Limbs were stabilized by either stiff fixation plates for the duration of the study or compliant plates that allowed transfer of compressive ambulatory loads beginning at week 4. Healing was assessed by digital radiography, microcomputed tomography, mechanical testing, histology, and finite element modeling. Loading significantly increased regenerate bone volume and average polar moment of inertia. The response to loading was location-dependent with the polar moment of inertia increased at the proximal end of the defect but not the distal end. As a result, torsional stiffness was 58% higher in the compliant plate group, but failure torque was not altered. In single samples assessed for histology from each group, a qualitatively greater amount of cartilage and a lesser degree of remodeling to lamellar bone occurred in the loaded group compared to the stiff plate group. Finally, principal strain histograms, calculated by FE modeling, revealed that the compliant plate samples had adapted to more efficiently distribute loads in the defects. Together, these data demonstrate that functional transfer of axial loads alters BMP-induced large bone defect repair by increasing the amount and distribution of bone formed within the defect. © 2011 Orthopaedic Research Society. Published by Wiley Periodicals, Inc. *J Orthop Res*

Keywords: mechanical loading; bone tissue engineering; bone defect; bone adaptation

Bone uniquely adapts and remodels its architecture and properties to respond to its mechanical environment, and mechanical forces are essential for proper morphogenesis and maintenance of normal bone structure and function.¹ Bone repair is also acutely responsive to loading, and both fracture healing and distraction osteogenesis are highly sensitive to mechanical stimuli, with the local mechanical environment being a primary determinant of the course and success of healing.^{2–3}

Although it was long held that complete immobilization was imperative for successful fracture healing and that the resorptive effect of disuse was necessary to release calcium for callus mineralization, the potential benefits of mechanical stimulation to bone repair are now well recognized.⁴ Continued study of the role of biomechanical factors during fracture healing has in fact significantly altered the clinical management of fractures.^{5–7} In particular, it is now known that limited compressive interfragmentary movements induce endochondral ossification and have a stimulatory effect on callus formation and subsequent healing.^{2,8–10}

Although biomechanical modulation of fracture healing has been well studied, the ability of mechanical stimulation to enhance large bone defect repair has not yet been quantitatively evaluated. Large bone

defects, caused by traumatic injury, tumor resection, or degenerative disease, remain a significant challenge for orthopedic surgeons, as the current treatment options are limited by tissue availability and donor site morbidity, in the case of autografts, and failure to revitalize and remodel, in the case of allografts.^{11–13} Tissue engineering, the use of biomaterial scaffolds in combination with biologics and/or cells, has therefore emerged as a promising alternative to grafting techniques. One tissue engineering strategy that shows immense potential is the delivery of recombinant osteoinductive growth factors, such as members of the bone morphogenetic protein (BMP) family. Two of these factors, BMP-2 and BMP-7, have been approved for use in humans by the United States Food and Drug Administration (FDA), and have shown great promise in numerous animal models and clinical trials.^{14–16} The clinical delivery method for these proteins, however, may be inefficient as large doses are required, contributing to prohibitively high costs and potential complications due to protein diffusion.^{14–15} A recently developed growth factor delivery system, using an alginate hydrogel injected into a nanofiber mesh tube placed around the defect, has been shown to enhance functional repair of bone defects.¹⁷ Such advances are increasing the potential to safely and effectively restore bone function in challenging segmental defects.

However, few studies have directly investigated the influence of mechanical conditions in tissue-engineered bone repair. While a number of laboratories have explored mechanical deformations of bone cells and tissue-engineered constructs in vitro,^{18–22} very few have

Additional Supporting Information may be found in the online version of this article.

The authors declare they have no conflicts of interest.

Correspondence to: Robert E. Guldberg (T: 404-385-6589; F: 404-894-2291; E-mail: robert.guldberg@me.gatech.edu)

© 2011 Orthopaedic Research Society. Published by Wiley Periodicals, Inc.

studied these *in vivo*,^{23–25} and the potential of mechanical loading to enhance the regeneration of large bone defects has not been evaluated. This approach has the potential to improve clinical treatment of such challenging defects as well as advance our understanding of the role of mechanical factors in bone tissue formation, differentiation, and remodeling. The aim of this study was therefore to test the hypothesis that transfer of compressive ambulatory loads during segmental bone repair enhances bone formation and subsequent limb regeneration.

METHODS

Surgical Procedure

Bilateral 6-mm femoral defects were surgically created in 13-week-old female SASCO Sprague–Dawley rats (Charles River Labs, Wilmington, MA) under isoflurane anesthesia as previously described.²⁶ Pilot studies were performed to verify that these defects were critically sized and bone bridging was not observed in empty defects (Supplementary Fig. 1A). Limbs were stabilized by either stiff or axially compliant fixation plates as characterized previously²⁷ ($n = 10$ per group, Fig. 1A–C). The compliant plates maintained a high stiffness to bending and torsional loads, but allowed transfer of compressive ambulatory loads through integrated elastomer segments (RTV Silicone Adhesive, Factor II, Inc., Lakeside, AZ) that conferred a low axial stiffness.²⁷ The compliant plates also featured a locking mechanism to allow elective actuation of load-sharing after an initial healing period, selected to be 4 weeks in the current study. In the locked configuration, the compliant plates featured an axial stiffness of 349.5 ± 35.1 N/mm, which was reduced to 8.4 ± 0.4 N/mm by plate actuation. By comparison, the stiff plates featured an axial stiffness of 214.3 ± 4.1 N/mm.²⁷ After limb

stabilization, a nanofiber mesh tube was inserted over the native bone ends, surrounding the defect.¹⁷ One hundred microliters of alginate hydrogel, containing $5 \mu\text{g}$ of BMP-2, was then injected into each mesh using a blunt-tipped 22 g needle, filling the defect space as previously described¹⁷.

Animals were given subcutaneous injections of 0.04 mg/kg buprenorphine every 8 h for the first 48 h post-surgery and 0.013 mg/kg every 8 h for the following 24 h. All procedures were reviewed and approved by the Georgia Institute of Technology Institutional Animal Care and Use Committee (Protocol No. A08032).

Nanofiber Mesh Production

Nanofiber meshes were produced as described previously by electrospinning poly-(ϵ -caprolactone) (PCL) onto a static collector.²⁸ Briefly, PCL was dissolved at a concentration of 12% (w/v) in a 90:10 volume ratio of hexafluoro-2-propanol:dimethylformamide (Sigma–Aldrich, St. Louis, MO) and electrospun onto a collector. Twenty-four 1 mm diameter perforations were patterned into the sheets, which were then glued into tubes of 4.5 mm diameter and 10 mm length. Mesh tubes were sterilized by 100% ethanol evaporation.

Alginate and Growth Factor Loading

Recombinant human BMP-2 (R&D Systems, Minneapolis, MN) was reconstituted in 0.1% rat serum albumin in 4 mM HCl, and mixed with RGD-functionalized alginate (courtesy of David Mooney, Harvard University)²⁹ to a final concentration of $50 \mu\text{g}/\text{ml}$ in 2% alginate. To crosslink the alginate, this solution was mixed rapidly with 0.84% (m/v) CaSO_4 . Each defect received a total of $5 \mu\text{g}$ BMP-2.

Faxitron and MicroCT

Two-dimensional digital radiographs (Faxitron MX-20 Digital; Faxitron X-Ray Corp., Wheeling, IL) were taken at 2, 4, 8, and 12 weeks post-surgery with an exposure time of 15 s and a voltage of 25 kV ($n = 10$ per group) (Table 1). *In vivo* micro-computed tomography (microCT) scans (Viva-CT 40; Scanco Medical, Basserdorf, Switzerland) were performed at 4, 8, and 12 weeks post-surgery at medium resolution and $38.5\text{-}\mu\text{m}$ isometric voxel size with the scanner set at a voltage of 55 kVp and a current of $109 \mu\text{A}$. The volume of interest (VOI) used for quantification of bone volume and bone density encompassed all bone formation within the center 100 slices (3.85 mm) between the native bone ends. New bone formation was segmented by application of a global threshold ($386 \text{ mg hydroxylapatite}/\text{cm}^3$) corresponding to 50% of the native cortical bone density, and a Gaussian filter ($\sigma = 1.2$, support = 1) was used to suppress noise.

After 12 weeks (8 weeks after compliant plate actuation), the animals were euthanized by CO_2 asphyxiation, and the

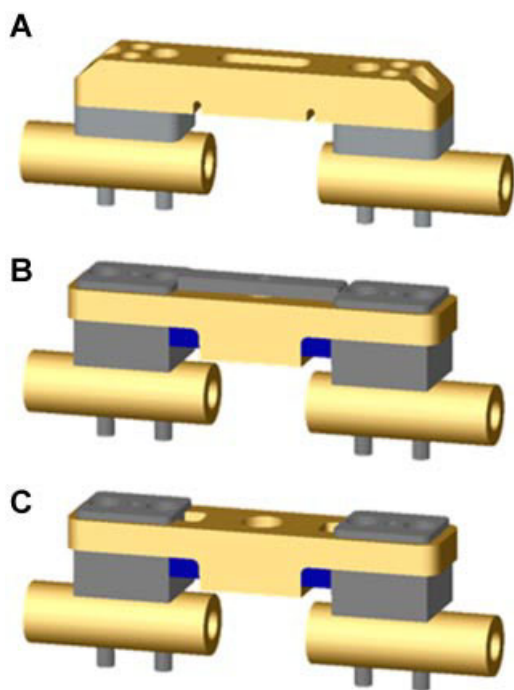


Figure 1. Fixation plate designs. (A) Stiff plate; (B) locked compliant plate; (C) actuated compliant plate.

Table 1. Analyses Performed and Sample Sizes for both Stiff and Compliant Plate Groups

Analysis Method	Time Points (Week)	N (per Group)
Faxitron	4, 8, 12	10
MicroCT	4, 8, 12	8
Mechanical Testing	12	8
Histology	5, 12	1
FE Modeling	12	3

limbs were excised for microCT scanning to quantify bone distribution ($n = 8$ per group). Ex vivo scans were performed as above at medium resolution with a 21- μm voxel size. The ex vivo VOI included the defect plus 2 mm of native bone on each end, to encompass the entire region exposed to a torsional moment during mechanical testing. To assess the cross-sectional bone distribution, the “Bone Midshaft” evaluation script (Scanco Medical, Basserdorf, Switzerland) was used to quantify polar moment of inertia (pMOI).

Biomechanical Testing

Femora ($n = 8$ per group) were then biomechanically tested in torsion to failure as described previously.²⁶ Briefly, limbs were cleaned of soft tissues and the ends potted in Wood’s metal (Alfa Aesar, Wood Hill, MA). The fixation plates were then removed, and limbs were mounted on a Bose Electro-Force system (ELF 3200, Bose EnduraTEC, Minnetonka, MN) and tested to failure at a rate of 3°/s. Maximum torque at failure and torsional stiffness, given by the slope of the line fitted to the linear region of the torque–rotation curve, were computed for each sample.

Histology

One sample per group was taken for histology at week 5 (1 week after compliant plate actuation) and at week 12 post-surgery. Samples were fixed in 10% neutral buffered formalin for 24 h at 4°C, and then transferred to a formic acid-based decalcifier (Cal-ExII; Fisher Scientific, Pittsburgh, PA) for 2 weeks, under mild agitation on a rocker plate. Following paraffin processing, 5 μm -thick mid-sagittal sections were cut and stained with Picrosirius red³⁰ and Safranin-O/Fast-green.³¹ Picrosirius red staining was performed to compare the local tissue organization and degree of cell-mediated remodeling between groups at weeks 5 and 12 post-surgery. When viewed under polarized light, the collagen fibers become birefringent and distinguish organized lamellar bone from unorganized woven bone. Cartilage areas in Safranin-O sections were segmented and evaluated by using a colorimetric threshold (Axiovision, Carl Zeiss, Germany). Manual contouring of lamellar and woven bone areas in ImageJ³² allowed comparison of organization and maturity in Picrosirius red sections.

Finite Element Modeling

MicroCT-generated reconstructions of three representative defects per group were subjected to finite element (FE) analysis following voxel to element conversion (voxel size: 42 μm), and the spatial and frequency distributions of maximum and minimum principal strains were determined under physiologic loads. Rat femoral loads caused by gravitational impact during ambulation have previously been estimated as one-half the body weight (BW);³³ however, there is increasing evidence that muscle contraction loads contribute significantly to adaptive signals.³⁴ Therefore, in vivo femoral loads, P_{femur} , were assumed to be axially oriented at a magnitude of 1.0 BW. Traction boundary conditions on the in-grown bone, P_{defect} , were then determined by the “rule of mixtures,” to account for load-sharing with the fixation plate:

$$P_{\text{defect}} = P_{\text{femur}} \times \frac{k_{\text{defect}}}{k_{\text{defect}} + k_{\text{plate}}} \quad 1$$

where k_i = axial stiffness of the i th species, and P_i = axial load on the i th species, for both stiff and compliant plate samples. A sensitivity study was conducted to evaluate the

effect of error in femoral load estimation on local mechanical conditions. The cortical bone ends were segmented and given a modulus of 10 GPa,³⁵ while the newly formed bone properties were determined by back-calculation from physical tests. The Poisson ratio was assumed to be 0.33.

To estimate a modulus for newly formed bone, separate samples were tested non-destructively in axial compression to an effective strain of 1,200 μstrain . Axial loads and effective defect strains, measured by laser extensometer (LX 500, MTS, Eden Prairie, MN), were used to determine axial stiffness (k_{actual}). Corresponding microCT reconstructions were subjected to the analogous FE analysis to yield an axial stiffness (k_{FE}) based upon an arbitrary elastic modulus ($E_{\text{FE}} = 2,000$ MPa). Linear correlation between measured and calculated stiffness values²³ provided the elastic tissue modulus,

$$E_{\text{actual}} = E_{\text{FE}} \times \frac{k_{\text{actual}}}{k_{\text{FE}}} \quad 2$$

Statistical Analyses

All data are presented as mean \pm standard error of the mean (SEM). Differences between groups, among time points, and among spatial regions, accounting for animal variability, were assessed by two- and three-factor analysis of variance (ANOVA), as appropriate (Minitab[®] 15, Minitab Inc., State College, PA). Individual comparisons were made by Tukey’s post hoc analysis. Comparison of regression lines was performed by analysis of covariance (ANCOVA). A p -value < 0.05 was considered significant.

RESULTS

Faxitron

Faxitron radiographs taken at weeks 4, 8, and 12 post-surgery confirmed that both stiff and compliant plates maintained limb stability, and the delivered growth factor induced bridging of the defects prior to compliant plate actuation at week 4, with bone completely filling the defect space by week 12 (Fig. 2).

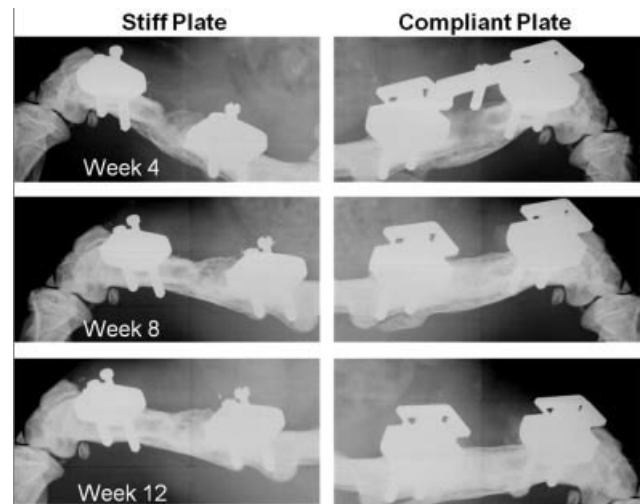


Figure 2. Faxitron radiographs taken at weeks 4, 8, and 12 post-surgery. The compliant plate was locked until plate actuation at week 4, followed by 8 weeks of functional loading.

MicroCT

In vivo microCT scans were performed every 4 weeks post-surgery. Prior to compliant plate actuation at week 4, the bone volume was not significantly different between groups; however, after 4 weeks of load transfer, at week 8, the compliant plate group featured a significantly greater bone volume than the stiff plate group, and this difference continued through week 12 (Fig. 3A). Though both groups featured a continuous increase in mean density throughout the experiment, there were no differences in mean density between groups at any time point (Fig. 3B). Three-dimensional reconstructions of the defects at week 12 demonstrated qualitative differences in bone distribution as a function of axial position (Fig. 3C), though the local density distribution within the defect did not change along the bone axis or between groups (Fig. 3D, data not shown).

Biomechanical Testing

Post mortem mechanical testing was performed to assess the degree of functional regeneration of the limbs. Torsion tests demonstrated a significant 58.2% increase in torsional stiffness as a result of compliant fixation (Fig. 4A); however, loading did not alter the maximum torque at failure (Fig. 4B) or the work to failure (data not shown).

Bone Distribution

Compliant fixation resulted in a significant 30.4% increase in average polar moment of inertia (pMOI, Fig. 5A). To quantify the location dependence of the bone distribution, the pMOI was graphed as a function of position from the defect center, x (Fig. 5B). In both groups, linear regression indicated a significantly positive slope in pMOI versus x (from distal to proximal end). The regression lines differed significantly, with the compliant plate group having both greater slope and intercept (Stiff: $m = 4.35 \pm 0.386$, $b = 56.69 \pm 1.05$, $R^2 = 0.7468$; Compliant: $m = 7.65 \pm 0.448$, $b = 66.2 \pm 1.22$, $R^2 = 0.8715$).

As each data set more closely approximated a triphasic curve, with inflection points at the native bone ends, the pMOI values were binned into three regions, determined by the edges of the defect (Fig. 5C). At the distal end, where the pMOI was a minimum, there was no significant effect of loading on bone distribution; however, in both the defect and proximal regions, loading significantly increased the bone distribution (Fig. 5D).

Histology

Comparison of lamellar and woven bone areas using picosirius red staining qualitatively revealed no

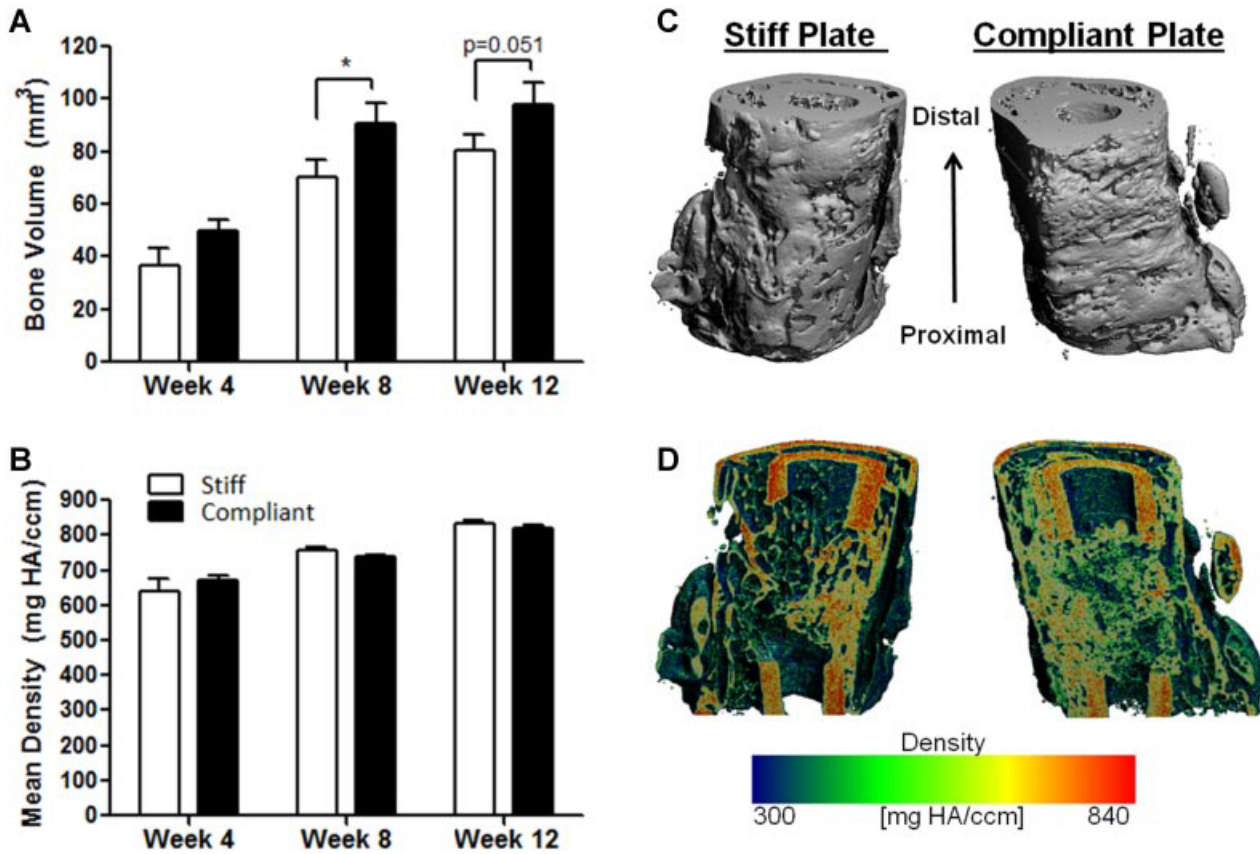


Figure 3. (A) Bone volume and (B) mean density at weeks 4, 8, and 12 post-surgery. Bone formation was significantly increased after 4 weeks of loading in the compliant plate group over the stiff plate group. (C) Representative 3-D reconstructions of limbs qualitatively demonstrated a difference in distribution between the proximal and distal ends of the defects. (D) Local density mapping on sagittal cross sections illustrated internal distribution and maturity.

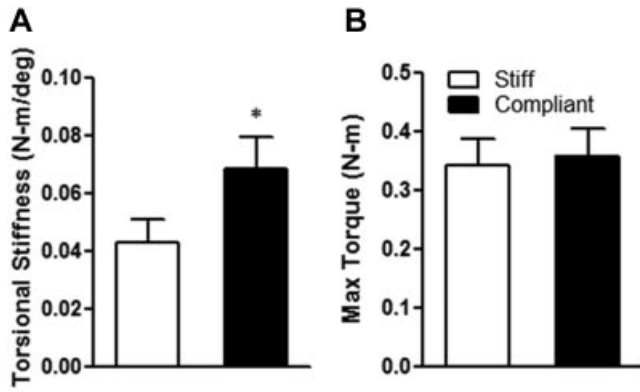


Figure 4. Torsional stiffness (A), but not maximum torque at failure (B), was significantly enhanced by compliant fixation.

differences between samples after 1 week of loading at week 5 (Fig. 6A and B); however, by week 12, the stiff plate sample had a greater proportion of lamellar bone, indicating a more remodeled architecture, while the compliant plate tissue appeared unchanged (Fig. 6C and D).

Safranin-O/Fast-green revealed positive staining for cartilage in both groups and at both time points (Fig. 7A–F). Cartilage appeared predominantly at the distal end of the defect, and very little cartilage staining was found near the proximal end (Fig. 7A and B). In the limited number of samples evaluated ($n = 1/\text{group and time point}$), Safranin-O staining qualitatively demonstrated a larger amount of cartilage in the compliant plate samples compared to the stiff plate samples. At week 5, hypertrophic chondrocytes were

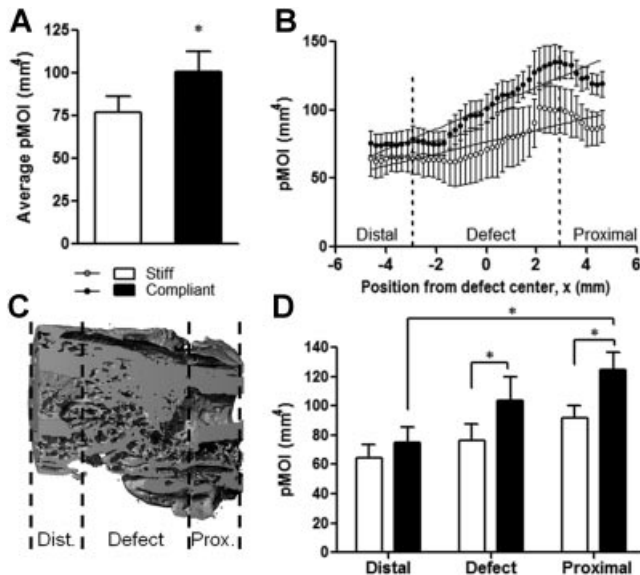


Figure 5. (A) MicroCT quantified a significantly greater average polar moment of inertia (pMOI) in the compliant plate group at week 12. (B) Graph of local pMOI versus distance from defect center quantitatively verified differences in distribution as a function of position. Also, the slopes of regression lines were significantly different between the two groups. (C) Illustration of regions used for binning data from B. (D) Comparison of average pMOI in each region, demonstrating no differences in distribution at the distal end where the pMOI was a minimum.

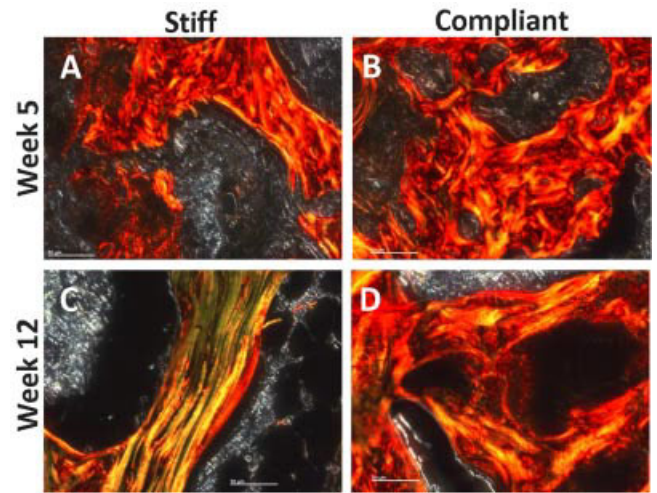


Figure 6. Picosirius red images, viewed under polarized light to highlight collagen I organization. (A) Stiff plate group at week 5. (B) Compliant plate group at week 5. (C) Stiff plate group at week 12. (D) Compliant plate group at week 12. Qualitatively, no differences were observed at week 5, 1 week after load initiation; however, a qualitatively greater proportion of lamellar bone was evident in the stiff plate group compared to the compliant plate group at week 12. Images are representative, selected based on average ratio of woven bone area:total bone area. Scale bars: 50 μm .

evident at the edges of cartilage islands and embedded in mineralized matrix, suggesting an endochondral ossification process (Fig. 7C and D). Comparatively, very few glycosaminoglycan (GAG)-secreting chondrocytes remained by week 12, and most remaining hypertrophic chondrocytes were fully surrounded by mineralized matrix (Fig. 7E and F). Alginate gel also stained red but was acellular and therefore easily identifiable (Fig. 7E and F).

Finite Element Modeling

Back-calculation of material properties from physical tests determined the average tissue modulus for regenerate bone at week 12 ($628.43 \pm 54.47 \text{ MPa}$). The in vivo defect loads, P_{defect} , were calculated to be 48% greater in the compliant plate group at week 12 (Stiff: $2.00 \pm 0.18 \text{ N}$; Compliant: $2.95 \pm 0.06 \text{ N}$, $p = 0.0072$). However, the resulting average principal strains were not different between the two groups (data not shown), which suggests an adaptive response in the compliant plate group to minimize overstrain by adding bone tissue. Accordingly, the apparent modulus of the compliant plate group was significantly increased over the stiff plate group (Stiff: $84.8 \pm 25.2 \text{ MPa}$; Compliant: $121.3 \pm 11.6 \text{ MPa}$, $p = 0.037$).

At week 12, the minimum and maximum principal strains ranged from approximately -500 to $300 \mu\text{strain}$, respectively, for both groups, but the frequency distribution of these strains throughout the defect was different between groups (Fig. 8). In the stiff plate group, a larger proportion of voxels carried very low strains (Fig. 8A); whereas, in the compliant plate group, strains were more evenly distributed (Fig. 8B). This effect is further illustrated in the representative

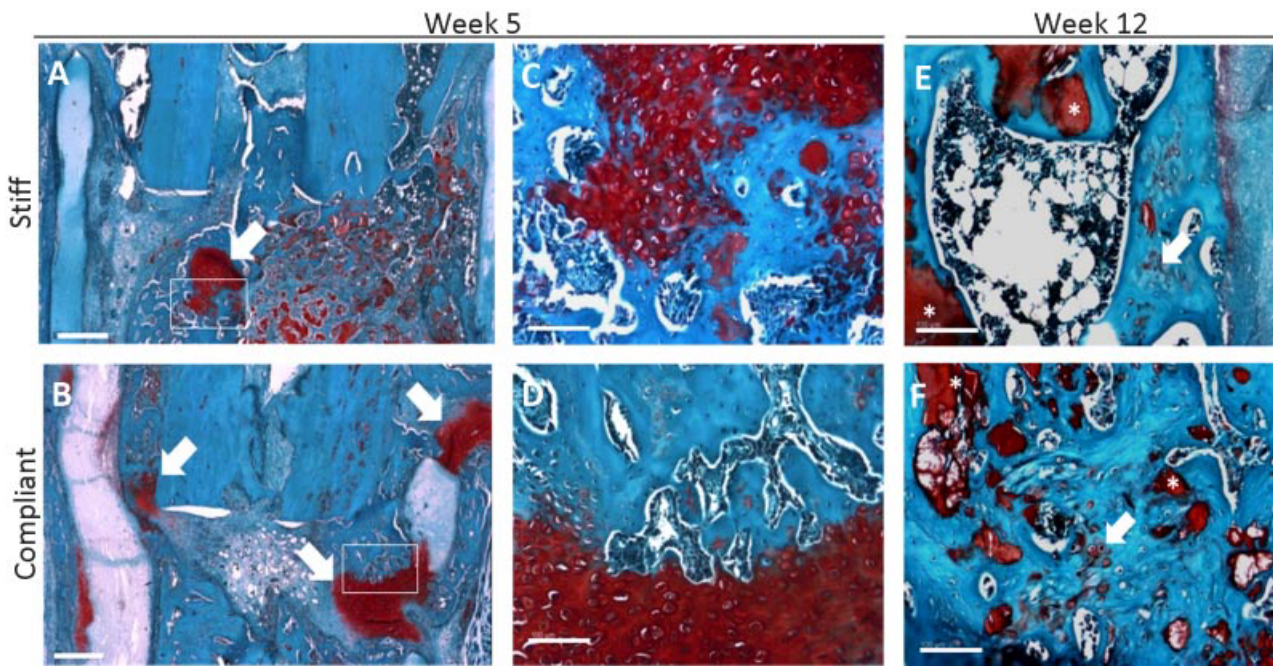


Figure 7. Safranin-O/Fast green images. (A,B) Cartilaginous tissue at distal end of stiff and compliant plate groups, respectively, at week 5. Scale bars: 500 μm . (C,D) Boxed areas from A and B, respectively, demonstrating hypertrophic chondrocytes and bone/cartilage interface. Scale bars: 100 μm . (E,F) Hypertrophic chondrocytes (white arrows) embedded in mineralized matrix from compliant and stiff plate groups, respectively, at week 12. Qualitatively, a greater amount of cartilage formation was found in the compliant plate group, and in all samples, cartilage formation occurred predominantly at the distal end of the defects. Scale bars: 100 μm .

minimum principal strain mapping images (Fig. 8C and D).

DISCUSSION

This study demonstrates that manipulation of fixation stiffness during the course of segmental bone defect healing significantly affects the amount, distribution, and biomechanical properties of regenerated bone within the defect. In this experiment, limbs were stabilized with either stiff plates or compliant plates designed to transfer axial loads to the ingrowing bone while resisting transfer of torsional and bending moments. Axial loading significantly increased bone formation and cross-sectional distribution, conferring a significant enhancement in elastic stiffness, but did not alter the maximum torque at failure or work to failure.

These observations may be explained by application of simple mechanics of materials theory to the distribution data. While loading significantly increased the average pMOI, it did not alter bone distribution at the distal end, where failure during biomechanical testing was observed. Assuming that the tissue modulus did not vary by position, the torsional stiffness is given by:

$$k_t = \frac{G \times J_{\text{avg}}}{L} \quad 3$$

where G is the elastic shear modulus, J_{avg} is the average pMOI, and L is the gage length of the test. Thus, an increase in average pMOI, induced by mechanical stimulation, would cause a proportional increase in

stiffness. Failure, however, occurs when the maximum shear stress reaches a critical value. The maximum shear stress in the limb is related, not to the average pMOI, but to the minimum pMOI by:

$$\tau_{\text{max}} = \frac{T \times r}{J_{\text{min}}} \quad 4$$

where T is the torque, and r is the outer radius at the location of J_{min} , the minimum pMOI. Since loading did not alter bone distribution at the distal end, where the pMOI was a minimum, the failure properties were not affected by loading.

For comparison, the mechanical properties of age-matched intact femurs were 0.030 ± 0.001 N-m/deg and 0.31 ± 0.02 N-m for torsional stiffness and failure torque, respectively.²⁷ A previous study using the same protein delivery system with 5 μg rhBMP-2 in 8 mm defects reached about 75% of intact bone properties for both stiffness and torque, though these were not statistically different from the native bone properties.³⁶ In this study, with a 6Ymm defect, the stiffness and failure torque of the stiff plate group were similar to intact bone; however, in the compliant plate group, the torsional stiffness was significantly greater than that of the unoperated limbs.

The observed axial variation in distribution, regardless of fixation type, may be due to a variation in vascular supply, which could affect the availability of osteoprogenitor cells. Given a sufficient vascular supply, mesenchymal stem cells (MSCs) can differentiate into bone forming osteoblasts; however, in hypoxic

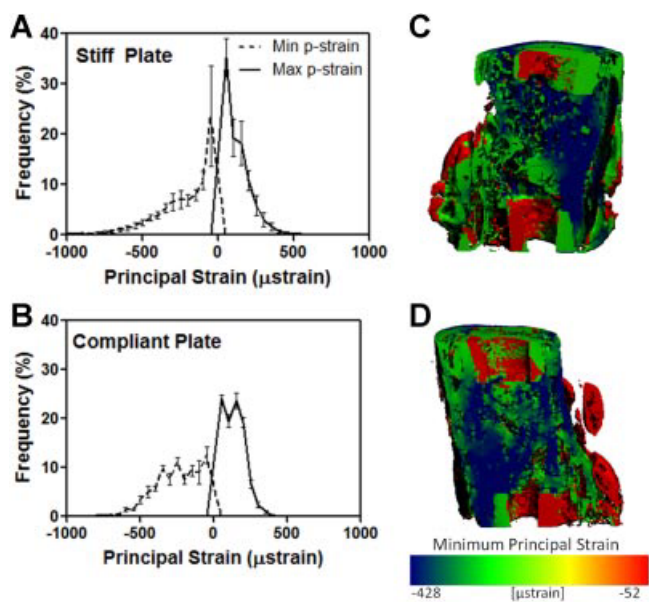


Figure 8. Finite element modeling of samples at week 12. (A,B) Superimposed maximum/minimum principal strain histogram for stiff and compliant plate groups, respectively. (C,D) Local minimum principal strain mappings for stiff and compliant plate groups, respectively. Despite a greater amount of load transfer in the compliant plate group, the average principal strains were not different between groups; however, the frequency distribution of the local strains was more evenly distributed in the compliant plate group.

environments, they may preferentially differentiate into chondrocytes.¹⁷ Accordingly, in this experiment, positive staining for cartilage was evident primarily at the distal end of the defects, suggesting locally reduced perfusion. Likewise, in agreement with the strain-mediated tissue differentiation theories proposed by Carter, Perren, and others, more cartilage was found in loaded samples, at both week 5 and week 12.^{1,37} This finding agrees with other *in vivo* model systems in which mechanical stimulation altered the tissue differentiation profile and prolonged the chondral phase of the endochondral ossification process.^{38–40}

RhBMP-2 can induce intramembranous or endochondral ossification, depending on various factors including anatomic location.^{41,42} Unlike the mechanical instability studies performed on bone fractures or non-critically sized osteotomies,^{7,10,40,43} these segmental bone defects did not display exuberant external callus formation in either group. The compliant fixation plates, while allowing axial load transfer, did not result in mechanical instability. However, we have found in a separate study that if the uniaxial constraint is removed, allowing multi-modal loading, these defects progress to non-union as a result of instability (data not shown). With stable plates (either stiff or axially compliant), formation of cartilage was inconsistent and a combination of intramembranous and endochondral bone formation occurred, though the mechanical stimulus may increase or prolong endochondral ossification.

The interactions between rhBMP-2 and mechanical loading were not directly investigated in this study.

BMP-2 mRNA expression increases in response to mechanical stimulation *in vitro*,^{20,44} and the effects of rhBMP-2 delivery to non-critically sized fractures depends upon mechanical conditions,⁴⁵ however, these interactions are not well understood, especially in large bone defects which require biologic treatment to heal. In this model, empty and nanofiber mesh-only defects filled with fibrous tissue resulting in non-union; therefore, a control group with loading but no rhBMP-2 was not included. However, unpublished preliminary data suggest that at lower doses of rhBMP-2 which do not induce bridging, an effect of loading is not apparent. Future work will address these potentially important interactions.

In addition to differences in tissue composition, the response to functional loading was location dependent, such that the proximal and defect regions experienced a significant increase in bone distribution as a result of loading, while the distal region was not affected. While a possible explanation is spatial inhomogeneity in the mechanical environment, principal strains were not different between the proximal and distal ends (data not shown). Therefore, this location-dependence may have been caused by a less favorable vascular environment for progenitor differentiation at the distal end, which would provide fewer mechanosensitive cells to respond to the local mechanical stimulus.

FE modeling allowed back-calculation of the local material properties of tissue-engineered bone. This value (628.43 ± 54.47 MPa) is substantially lower than reported values for rat cortical bone, which are on the order of 10 GPa,³⁵ but is very similar to the reported tissue modulus of woven bone (approximately 600 MPa).²³ While the boundary conditions were calculated based on femoral loads equal to the body weight, a sensitivity analysis assuming one order-of-magnitude error in boundary conditions yielded corresponding 10-fold differences in strain magnitude, but did not affect the strain distribution patterns presented. The flattening of the frequency distribution curve in the compliant plate group indicates that strains are distributed over more voxels, suggesting that these samples had adapted to more efficiently carry the applied loads.

The FE modeling assumed that mechanical loading did not alter the local elastic properties of the tissue. While the mean density was not affected by loading, load-mediated adaptive modeling did alter the microstructural maturity. Collagen organization demonstrated that loading prolonged the presence of woven bone. This finding suggests a possible reduction in the tissue-level material properties of the loaded samples, as lamellar bone has a higher tissue modulus than woven bone,²³ and would accentuate the observed differences in local strains and structural properties between groups. This load magnitude-dependent modulation of bone maturity has been observed previously,²³ and could result from increased or prolonged osteoblast activity or reduced osteoclast activity.

An additional limitation of the microCT-based approach is that only mineralized tissues can be evaluated. Therefore, the soft tissue inhomogeneities including cartilage and fibrous tissue were not included in the FE models or moment of inertia calculations, which modeled non-mineralized matrix as voids. However, at the time point of FE modeling, MOI analysis, and mechanical testing, week 12, the amount of cartilage in the defects was minimal and therefore not likely to dominate the behavior. Likewise, the differences in modulus between these soft tissues and bone further suggest that the mineralized matrix is likely the primary contributor to the structural properties. Similarly, the simple mechanics of materials analysis did not include the inhomogeneity of the tissue. However, this procedure was not performed to determine values, but rather to mathematically explain the experimental observations that an increase in average polar moment of inertia led to increases in stiffness, while the lack of change in minimum moment of inertia resulted in no differences in maximum torque. Therefore, despite the above simplifications, this analysis qualitatively explained these observations.

In conclusion, this study demonstrated that functional transfer of axial loads by modulation of fixation plate stiffness significantly altered BMP-mediated large bone defect repair by increasing bone formation and distribution and modulating tissue organization and differentiation. Defect stiffness was increased, but structural strength was not altered. Consideration of the mechanical environment may therefore improve clinical treatment of challenging segmental bone defects and advance our understanding of the role of biomechanical factors in bone tissue differentiation, formation, and remodeling.

ACKNOWLEDGMENTS

This study was supported by NIH grant AR051336. We would like to thank the following individuals: Dr. David Mooney, for providing the RGD-Alginate, Dr. Laura O'Farrell, for assistance with animal studies, and Sha'aqua Asberry for assistance with histology. We gratefully acknowledge Dr. Tamim Diab, Brent Uhrig, Dr. Mela Johnson, Christopher Dosier, and Jessica O'Neal for their assistance in surgery.

REFERENCES

1. Carter DR, Van Der Meulen MC, Beaupre GS. 1996. Mechanical factors in bone growth and development. *Bone* 18:5S-10S.
2. Goodship AE, Kenwright J. 1985. The influence of induced micromovement upon the healing of experimental tibial fractures. *J Bone Joint Surg Br* 67:650-655.
3. Richards M, Goulet JA, Weiss JA, et al., 1998. Bone regeneration and fracture healing. Experience with distraction osteogenesis model. *Clin Orthop Relat Res* 355 Suppl: S191-S204.
4. Baker AH. 1934. Non-union in fractures. *Ulster Med J* 3:277-283.

5. Yamagishi M, Yoshimura Y. 1955. The biomechanics of fracture healing. *J Bone Joint Surg Am* 37-A:1035-1068.
6. Kenwright J, Richardson JB, Cunningham JL, et al., 1991. Axial movement and tibial fractures. A controlled randomised trial of treatment. *J Bone Joint Surg Br* 73:654-659.
7. Epari DR, Kassi JP, Schell H, et al., 2007. Timely fracture-healing requires optimization of axial fixation stability. *J Bone Joint Surg Am* 89:1575-1585.
8. Claes L, Augat P, Schorlemmer S, et al., 2008. Temporary distraction and compression of a diaphyseal osteotomy accelerates bone healing. *J Orthop Res* 26:772-777.
9. Klein P, Schell H, Streitparth F, et al., 2003. The initial phase of fracture healing is specifically sensitive to mechanical conditions. *J Orthop Res* 21:662-669.
10. Epari DR, Taylor WR, Heller MO, et al., 2006. Mechanical conditions in the initial phase of bone healing. *Clin Biomech (Bristol, Avon)* 21:646-655.
11. Sasso RC, LeHuec JC, Shaffrey C. 2005. Iliac crest bone graft donor site pain after anterior lumbar interbody fusion: a prospective patient satisfaction outcome assessment. *J Spinal Disord Tech* 18:S77-S81.
12. Koefoed M, Ito H, Gromov K, et al., 2005. Biological effects of rAAV-caAlk2 coating on structural allograft healing. *Mol Ther* 12:212-218.
13. Berrey BH Jr, Lord CF, Gebhardt MC, et al., 1990. Fractures of allografts. Frequency, treatment, and end-results. *J Bone Joint Surg Am* 72:825-833.
14. Einhorn TA. 2003. Clinical applications of recombinant human BMPs: early experience and future development. *J Bone Joint Surg Am* 85-A:82-88.
15. Mroz TE, Wang JC, Hashimoto R, et al., 2010. Complications related to osteobiologics use in spine surgery: a systematic review. *Spine (PhilaPa)* 35 (9 Suppl): S86-S104.
16. Axelrad TW, Einhorn TA. 2009. Bone morphogenetic proteins in orthopaedic surgery. *Cytokine Growth Factor Rev* 20:481-488.
17. Kolambkar YM, Dupont KM, Boerckel JD, et al., 2011. An alginate-based hybrid system for growth factor delivery in the functional repair of large bone defects. *Biomaterials* 32:65-74.
18. Matziolis G, Tuischer J, Kasper G, et al., 2006. Simulation of cell differentiation in fracture healing: mechanically loaded composite scaffolds in a novel bioreactor system. *Tissue Eng* 12:201-208.
19. Tanaka SM, Sun HB, Roeder RK, et al., 2005. Osteoblast responses one hour after load-induced fluid flow in a three-dimensional porous matrix. *Calcif Tissue Int* 76:261-271.
20. Rath B, Nam J, Knobloch TJ, et al., 2008. Compressive forces induce osteogenic gene expression in calvarial osteoblasts. *J Biomech* 41:1095-1103.
21. Ignatius A, Blessing H, Liedert A, et al., 2005. Tissue engineering of bone: effects of mechanical strain on osteoblastic cells in type I collagen matrices. *Biomaterials* 26:311-318.
22. Mauney JR, Sjostrom S, Blumberg J, et al., 2004. Mechanical stimulation promotes osteogenic differentiation of human bone marrow stromal cells on 3-D partially demineralized bone scaffolds in vitro. *Calcif Tissue Int* 74:458-468.
23. Guldberg RE, Caldwell NJ, Guo XE, et al., 1997. Mechanical stimulation of tissue repair in the hydraulic bone chamber. *J Bone Miner Res* 12:1295-1302.
24. Case ND, Duty AO, Ratcliffe A, et al., 2003. Bone formation on tissue-engineered cartilage constructs in vivo: effects of chondrocyte viability and mechanical loading. *Tissue Eng* 9:587-596.
25. Duty AO, Oest ME, Guldberg RE. 2007. Cyclic mechanical compression increases mineralization of cell-seeded polymer scaffolds in vivo. *J Biomech Eng* 129:531-539.

26. Oest ME, Dupont KM, Kong HJ, et al., 2007. Quantitative assessment of scaffold and growth factor-mediated repair of critically sized bone defects. *J Orthop Res* 25:941–950.
27. Boerckel JD, Dupont KM, Kolambkar YM, et al., 2009. In vivo model for evaluating the effects of mechanical stimulation on tissue-engineered bone repair. *J Biomech Eng* 131:084502.
28. Kolambkar YM, Peister A, Ekaputra AK, et al., 2010. Colonization and osteogenic differentiation of different stem cell sources on electrospun nanofiber meshes. *Tissue Eng* 16: 3219–3230.
29. Alsberg E, Kong HJ, Hirano Y, et al., 2003. Regulating bone formation via controlled scaffold degradation. *J Dent Res* 82:903–908.
30. Junqueira LC, Bignolas G, Brentani RR. 1979. Picrosirius staining plus polarization microscopy, a specific method for collagen detection in tissue sections. *Histochem J* 11:447–455.
31. Rosenberg L. 1971. Chemical basis for the histological use of safranin O in the study of articular cartilage. *J Bone Joint Surg Am* 53:69–82.
32. Abramoff MD, Magelhaes PJ, Ram SJ. 2004. Image processing with ImageJ. *Biophotonics Int* 11:36–42.
33. Clarke KA. 1995. Differential fore- and hindpaw force transmission in the walking rat. *Physiol Behav* 58:415–419.
34. Robling AG. 2009. Is bone's response to mechanical signals dominated by muscle forces? *Med Sci Sports Exerc* 41:2044–2049.
35. Oxlund H, Andersen NB, Ortoft G, et al., 1998. Growth hormone and mild exercise in combination markedly enhance cortical bone formation and strength in old rats. *Endocrinology* 139:1899–1904.
36. Kanichai M, Ferguson D, Prendergast PJ, et al., 2008. Hypoxia promotes chondrogenesis in rat mesenchymal stem cells: a role for AKT and hypoxia-inducible factor (HIF)-1 α . *J Cell Physiol* 216:708–715.
37. Perren SM, Cordey J, editors. 1980. The concept of interfragmentary strain. Current concepts in internal fixation of fractures.
38. Palomares KT, Gleason RE, Mason ZD, et al., 2009. Mechanical stimulation alters tissue differentiation and molecular expression during bone healing. *J Orthop Res* 27:1123–1132.
39. Cullinane DM, Fredrick A, Eisenberg SR, et al., 2002. Induction of a neoarthrosis by precisely controlled motion in an experimental mid-femoral defect. *J Orthop Res* 20:579–586.
40. Epari DR, Schell H, Bail HJ, et al., 2006. Instability prolongs the chondral phase during bone healing in sheep. *Bone* 38:864–870.
41. Yu YY, Lieu S, Lu C, et al., 2010. Bone morphogenetic protein 2 stimulates endochondral ossification by regulating periosteal cell fate during bone repair. *Bone* 47:65–73.
42. Stoeger T, Proetzel GE, Welzel H, et al., 2002. In situ gene expression analysis during BMP2-induced ectopic bone formation in mice shows simultaneous endochondral and intramembranous ossification. *Growth Factors* 20:197–210.
43. Lienau J, Schell H, Duda GN, et al., 2005. Initial vascularization and tissue differentiation are influenced by fixation stability. *J Orthop Res* 23:639–645.
44. Rui YF, Lui PP, Ni M, et al., 2011. Mechanical loading increased BMP-2 expression which promoted osteogenic differentiation of tendon-derived stem cells. *J Orthop Res* 29:390–396.
45. Cuenca-Lopez MD, Peris JL, Garcia-Rosello M, et al., 2010. Action of recombinant human BMP-2 on fracture healing in rabbits is dependent on the mechanical environment. *J Tissue Eng Regen Med* 4:543–552.